

Type-Specific Analysis of Morphometry of Dendrite Spines of Mice

E. Ceyhan^{1*}, L. Fong², T. N. Tasky³, M. K. Hurdal⁴, M. F. Beg⁵, M. E. Martone², J. T. Ratnanather^{3,6}

¹*Dept. of Mathematics, Koç University, 34450, Sarıyer, Istanbul, Turkey.*

*corresponding author: phone: +90 (212) 338-1845, fax: +90 (212) 338-1559,
email: elceyhan@ku.edu.tr, web: <http://home.ku.edu.tr/~elceyhan>

²*Dept. of Neurosciences, University of California, San Diego, CA, 92093, USA.*

³*Center for Imaging Science, The Johns Hopkins University, Baltimore, MD, 21218, USA.*

⁴*Dept. of Mathematics, Florida State University, Tallahassee, FL 32306-4510, USA.*

⁵*School of Engineering Science, Simon Fraser University, Burnaby, BC, V5A 1S6, Canada.*

⁶*Institute for Computational Medicine, The Johns Hopkins University, Baltimore, MD, 21218, USA.*

Abstract

In this article, we analyze the morphometric measures of dendrite spines of mice derived from electron tomography images for different spine types based on pre-assigned categories. The morphometric measures we consider include the metric distance, volume, surface area, and length of dendrite spines of mice. The question of interest is how these morphometric measures differ by condition of mice; and how the metric distance relates to volume, surface area, length, and condition of mice. The Large Deformation Diffeomorphic Metric Mapping algorithm is the tool we use to obtain the metric distances that quantize the morphometry of binary images of dendrite spines with respect to a template spine. We demonstrate that for the raw scores (i.e., values not adjusted for scale) metric distances and other morphometric measures are significantly different between the conditions. Furthermore, the morphometric measures (rather than the mice condition) explain almost all the variation in metric distances. Since size (or scale) dominates the other variables in variation, differences in metric distances due to other variables might be masked. Hence, we adjust metric distances and other morphometric measures for scale. We demonstrate that after adjusting for scale, scaled metric distances and other scaled morphometric variables still differ for condition, and scaled metric distances depend on most significantly on scaled morphometric measures. Although the methodology used here is applied on morphometric measures of dendrite spines, it is also valid for morphometric measures of other organs or tissues and other metric distances.

1. Introduction

The *Large Deformation Diffeomorphic Metric Mapping* (LDDMM) is a recently developed tool that quantizes morphometric (shape and size related) differences between two binary images. This approach has been applied to the analysis of gross brain morphology derived from magnetic resonance imaging

([2]; [21]; [32]; [15]; [16]). Here, we apply this technique to the quantification of shape changes of microscopic structures, the tiny protuberances found on many types of neurons termed *dendritic spines*. Changes in dendritic spine size, shape, and number are thought to underlie the brain's ability to change as a result of environmental stimulation and occur in many pathological conditions. Thus, the quantification of shape changes in dendritic spines is a fundamental problem in neuroscience. A previous version of this data (with fewer dendrite spines) was analyzed in ([1]) wherein a linear model was fit on metric distances versus other variables such as volume, surface area, and length values. In ([1]), statistical analyses were performed on metric distances and condition only. The dendritic spines were not matched for size and type of spine, so such factors might have caused the group differences in the metric distances, rather than the condition. Hence, other variables were included in the analysis. This same data set is also analyzed in ([7]), where the influence of the condition, spine type, volume, surface area, and length of spines on the metric distances was analyzed using a Principal Component Analysis (PCA). In this article, we analyze the morphometric measures of dendrite spines for each spine category, and model the metric distances with respect to other variables (volume, surface area, length, condition, mouse, spine number, and shaft label).

Methods developed in the field of *Computational Anatomy* (CA) that enable quantification of anatomical volumes and shapes between and within groups of individuals with and without various neurological diseases have emerged from several groups in recent years ([9]; [13]; [20]; [22]; [28]; [29]; [30]). Based on the mathematical principles of general pattern theory ([6]; [13]), these methods combine diffeomorphic maps between images with representations of anatomical shapes as smooth manifolds.

An important task in CA is the study of neuro-anatomical variability ([13]). The anatomic model is a quadruple $(\Omega, \mathcal{G}, \mathcal{I}, \mathcal{P})$ consisting of Ω the tem-

plate coordinate space (in \mathbb{R}^3), defined as the union of 0, 1, 2, 3-dimensional manifolds, $\mathcal{G} : \Omega \leftrightarrow \Omega$ a set of diffeomorphic transformations on Ω , \mathcal{I} the space of anatomies, is the orbit of a template anatomy I_0 under \mathcal{G} , and \mathcal{P} the family of probability measures on \mathcal{G} . In this framework, a geodesic $\phi : [0,1] \rightarrow \mathcal{G}$ is computed where each point $\phi_t \in \mathcal{G}, t \in [0,1]$ is a diffeomorphism of the domain Ω . The evolution of the template image I_0 along path ϕ is given by $\phi_t I_0 = I_0 \circ \phi_t^{-1}$ such that the end point of the geodesic connects the template I_0 to the target I_1 via $I_1 = \phi_1 I_0 = I_0 \circ \phi_1^{-1}$. Thus; anatomical variability in the target is encoded by these geodesic transformations when a template is fixed.

Furthermore, geodesic curves induce metric distances between the template and the target shapes in the orbit. The diffeomorphisms are constructed as a flow of ordinary differential equations $\dot{\phi}_t = v_t(\phi_t)$, $t \in [0,1]$ with $\phi_0 = id$ the identity map, and associated vector fields v_t , $t \in [0,1]$. The optimal velocity vector field parameterizing the geodesic path is found by solving

$$\hat{v} = \arg \inf_{v: \phi = \int_0^1 v_t(\phi_t) dt, \phi_0 = id} \int_0^1 \|v_t\|_V^2 dt \text{ such that } I_0 \circ \phi_1^{-1} = I_1$$

where $v_t \in V$, the Hilbert space of smooth vector fields with norm $\|\cdot\|_V$ defined through a differential operator enforcing smoothness. The length of the minimal geodesic path through the space of transformations connecting the given anatomical configurations in I_0 and I_1 defines a metric distance, D , between anatomical shapes in I_0 and I_1 via

$$D(I_0, I_1) = \int_0^1 \|\hat{v}_t\|_V dt$$

where \hat{v}_t is the optimizer calculated from the LDDMM algorithm ([3]). The construction of such a metric space allows one to quantify similarities and differences between anatomical shapes in the orbit. This is the vision laid out by D'Arcy W. Thompson almost one hundred years ago ([27]).

The notion of mathematical biomarker in the form of metric distance can be used in different ways. One way is to generate metric distances of shapes relative to a template ([24]; [3]). Another way is to generate metric distances between each shape

within a collection ([23]). The latter approach allows for sophisticated pattern classification analysis but is computationally expensive. We adopt the former approach here.

Previously, in ([1]) we demonstrated that almost all of the variation in the metric distances could be explained by $V^{1/3}$, $S^{1/2}$ and L where V , S , and L are volume, surface area, and length, respectively. That is, the size of the dendrites was shown to have the largest effect on the metric distances. However, when data was scaled, the condition was significant after accounting for scaled V , S , and L , and type of spine. In ([7]), we first considered the PCA on the numerical morphometric variables (V , S , and L), then used multiple linear regression on metric distances versus the principal components and other (categorical) variables. We demonstrate that the size component explains almost all the variation in the metric distances rendering the effect of condition insignificant. Since spine type is based on the size and shape of the dendrite spines, the morphometry of the spines at each spine category is (expected to be) more uniform than spines at different categories. Hence we analyze the morphometric features of dendrite spines at each spine type category.

2. Data acquisition

Pyramidal cells from layer V of primary visual cortex from genetically modified and control mice were injected with Lucifer yellow. Tissue was subsequently photo-oxidized and prepared for electron microscopy. 411 triangulated surface reconstructions of spine dendrites were produced by manual contouring of tomographic reconstructions of neurons and curated at the Cell-Centered DataBase at <https://ccdb.ucsd.edu/CCDB/index.shtml> ([18], [19]). The reconstructed spines were aligned with a standard coordinate system with respect to the smallest *Wild Type* (WT) spine via similitude matching (scale or no-scale, rotation, translation) of 14 landmarks suitably placed on each spine. LDDMM was applied to binarized images of the surfaces from which metric distances between the spines and the template (reference) spine were generated ([3]).

The variables we consider include spine number, mouse label, shaft label, condition, volume (V), surface area (SA), metric distance (D) values, length (L), scale (Sc) values, and classification category (i.e., type of spines). *Mouse Label* refers to labeling of each of 7 mice in the study; *Shaft label* refers to the shaft label for the associated mice; *Spine Number* refers to the spine associated with the shaft; *Condition of Mice* refers to whether the spine originated

from a WT mouse or a genetically modified mouse. The WT mice are expected to have a normal genetic make-up because they originate from natural mice populations. However, in the *Knock-Out* (KO) mice, one specific gene is inactivated in order to mimic a human neurological condition. The six spine types are *Double*, *Filopodia*, *Long Mushroom*, *Mushroom*, *Stubby*, and *Thin* ([14]). L is the Euclidean distance between the neck landmark at the point closest to the dendrite shaft and the head landmark at the point furthest from the dendrite shaft and is measured in μm (micron or micrometer); V is measured in μm^3 , and SA in μm^2 . Furthermore, scale (Sc) is the scale of mice with respect to the template spine obtained from similitude matching ([31]).

3. Results

3.1. Analysis of Unscaled Morphometric Measures

First, we analyze the unscaled numerical variables, namely, D , V , SA , and L measures and Sc values of dendrite spines. Since all of these variables are significantly non-normal ($p_L < .0001$ for each variable where p_L stands for Lilliefors's test of normality ([26])), we use Kruskal-Wallis (K-W) test ([8]) for the (distributional) equality of each of the morphometric variables (i.e., D , V , SA , and L measures and Sc values) between the spine type categories. We find that there are significant differences in each of these variables between the spine type categories (the p -value based on K-W test is $p_{KW} < .0001$ for each variable).

Among 411 spines, 225 are pre-assigned to type *Thin*, 59 to type *Mushroom*, 44 to type *Filopodia*, 31 to type *Long Mushroom*, 25 to type *Stubby*, and 4 to type *Double*; however 23 are not pre-assigned to any category. As there are too few *Double* type spines, the statistical tests involving *Double* spines will have virtually no power; hence we only investigate the morphometry of the other spine type categories. At each spine type category, the standard deviations of the morphometric measures (i.e., D , V , SA , L) for KO and WT mice have different order for spine type levels. See Table 1 for the p -values from Brown-Forsythe (B-F) equality or homogeneity of variances (HOV) tests ([16] C.B. Kirwan, C. Jones, M.I. Miller, C.E.L. Stark, "High-resolution fMRI investigation of the medial temporal lobe", *Human Brain Mapping*, 2007, (in press).

) and the direction of the alternatives. Significant p -values at .05 level are marked with an asterisk (*). Observe that HOV is not rejected for Sc values at each spine type category. When significant, (ℓ) alternative implies that the variance of KO spines are

significantly smaller than that of WT spines; i.e., there is less variation in the morphometry (shape and size) of KO spines compared WT spines; and vice versa for the (g) alternative. Notice also that most variation in the morphometry occurs for *Thin* spines, least variation occurs for *Mushroom* type spines, and the variable with most significant variation is V (significant for three spine types).

The following variables are significantly non-normal based on Lilliefors's test of normality: D , V , SA , and Sc for KO and WT *Thin* dendrite spines; Sc for WT, V and L for KO *Mushroom* type dendrite spines; V and SA for KO *Filopodia* type dendrite spines; D and L for KO *Long Mushroom* type dendrite spines; and V and SA for KO *Stubby* dendrite spines. Normality is not rejected for the other variables at $\alpha = .05$ level. Based on lack of HOV for some variables (see Table 1) and non-normality of most of the variables, we resort to the non-parametric Wilcoxon rank sum test to compare the variables for KO vs WT mice ([10]). The p -values and the direction of the alternatives are provided in Table 2 where significant p -values at .05 level are marked with an asterisk (*). Notice that D , V , SA , and L values for KO mice are significantly larger than those for WT mice at each spine type category (except for D for *Stubby* spines). That is, KO mice are significantly larger and longer in size and more different from the template spine in morphometry compared to WT mice. On the other hand, Sc values are significantly smaller for KO mice than WT mice (except for *Stubby* mice). That is, KO mice are closer in scale to the template spine than the WT mice.

Next, we will run ANOVA on D versus other variables (V , SA , L , Sc , spine, condition, mouse, and shaft type) one variable at a time at each spine type level. See Figure 1 for the pair plots between these numerical variables (D , V , SA , and $1/Sc$) with all the spines combined. The pair plots of the variables at each spine type (not presented) are similar. Observe that all the variables seem to be highly (positively) correlated with each other. But two of the major assumptions for linear models (and ANOVA) are the normality of errors and lack of autocorrelation between the errors. We have shown above that most of the variables are significantly non-normal. We transform the variables (and remove the few outliers if any) so that the variables satisfy normality and lack of autocorrelation. See Table 3 for the transformations. The transformed variables can be assumed to be normal ($p_L > .05$ for each) ([26]). For the kernel density plots of the raw and transformed variables, for e.g. *Mushroom* type spines, see Figure 2. Observe that the kernel density plots for the transformed variables look like normal density curves. The kernel

density plots of the raw and transformed variables are similar for other spine type categories (not presented).

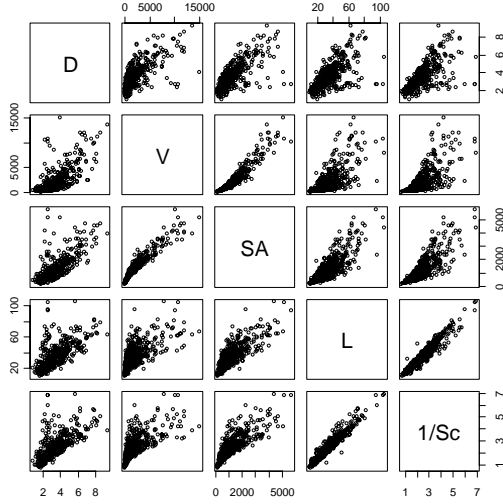


Figure 1: The pair plots of the morphometric measures (D , V , SA , and $1/Sc$) of the dendrite spines for all the spine types categories combined.

To determine which variables significantly explain the variation in metric distances, we run a linear model with tD being the response and each transformed variable being a predictor, one variable at a time. We record the variables that significantly explain the variation in tD measures (when included in the model one at a time) at each spine type category and present them in Table 3 in decreasing order of significance. Observe that shaft and spine variables are significant only for Thin spines, while the transformed morphometric (numerical) variables are significant for all spine types. Each significant variable at $\alpha=.05$ level is retained for further consideration, while others are discarded from the model.

At each spine type category, we run a linear model for which tD is the response variable, while all other variables that were found to be significant (see Table 4) with all possible interactions as predictor variables. On this full model we choose a reduced model by *Akaike information criteria* (AIC) in a *stepwise algorithm*, then use a *stepwise backward elimination procedure* on the resulting model ([5]). We stop the elimination procedure when all the remaining variables are significant at $\alpha = .05$ level. The resulting models for each spine type are provided in Table 5, where tD_{ij} is the distance for spine j for type i ($i=1$ for Thin, 2 for Mushroom, 3 for Filopodia, 4 for Long Mushroom, and 5 for Stubby), μ_i is the

overall mean for spines of type i , X_{ij}^{tSA} is the tSA value for spine j of type i , X_{ij}^{tSc} is the tSc value for

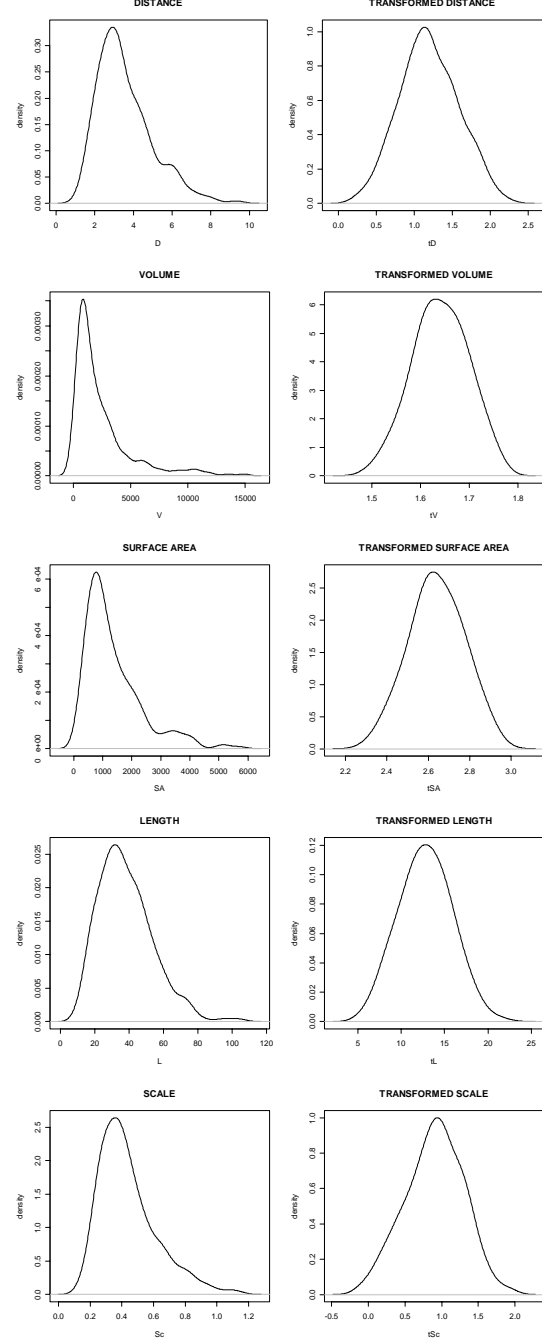


Figure 2: The kernel density estimates of raw D , V , SA , and Sc values (left) and of tD , tV , tSA , and tSc values (right) for Mushroom type spines.

spine j of type i , X_{ij}^{tV} is the tV for spine j of type i , β_i^{tSA} is the slope for tSA for spine type i , β_i^{tV} is the slope for tV for spine type i , β_i^{tSc} is the slope for tSc value for spine type i , and ε_{ij} is the error term.

The adjusted R^2 values and p -values based on Shapiro-Wilk normality test and Durbin-Watson autocorrelation test ([25]), denoted as p_{SW} and p_{DW} , respectively, are also provided in Table 5. Observe that the best predictors are tSA and tSc for Thin spines; tV for Mushroom and Filopodia spines; tSA for Long Mushroom spines; and tSc for Stubby spines. Therefore, tSA , tV , tSc , (i.e., size components) explain almost all of the variation in metric distances (e.g., 82 % for Mushroom type spines). However, differences in shape could be masked by the size of the dendrite spines. Note also that the normality of the errors is attained for all spine types except Thin spines, despite the transformations and removal of outliers. Hence, we estimate the significance of tSA , tSc , and condition variable by bootstrapping with 1000000 replicates ([11]) and obtain $p < .00001$, $p = .0041$, and $p = .5328$ for tSA , tSc , and condition, respectively. So the model for Thin spines in Table 5 is appropriate.

3.2. Analysis of Scaled Morphometric Measures

To overcome the highly dominant effect of size, we adjust the morphometric measures by scaling the dendrite spines and measure the D , V , SA , and L values for the scaled spines. For example, we obtain the scaled metric distances by applying the LDDMM algorithm to the scaled data (spines) rather than the distances that could be construed by scaling all the metric distances.

We consider the scaled numerical variables, namely, scaled metric distance (sD), scaled volume (sV), scaled surface area (sSA), and scaled length (sL) measures and the scale (Sc) values together with the categorical variables. After scaling, sD and sSA are more of shape measures, and sV and sL are expected to be more uniform compared to the unscaled versions. Since all of the numerical variables are significantly non-normal ($p_L < .0001$ for each), we employ K-W test and find that there are significant differences in each of these scaled variables between the spine type categories ($p < .0001$).

At each spine type category, we perform B-F test for HOV of the variables for KO and WT mice. The resulting p -values and the direction of the alternatives are provided in Table 6 where significant p -values at $\alpha = .05$ level are marked with an asterisk (*). Observe

that after scaling, HOV is rejected for sL of Thin and Filopodia spines, for sSA of Filopodia and Stubby spines, and for sV of Stubby spines. Furthermore, after scaling the morphometric measures obtain less spread or variation (see Tables 1 and 6), because the size variation is partly removed by scaling.

The following variables are significantly non-normal based on Lilliefor's test of normality: sV , sSA , and sL for KO Thin dendrite spines and sD , sV , and sSA for WT Thin dendrite spines; and sV for WT Long Mushroom type dendrite spines. Normality is not rejected for the other variables at .05 level. Notice that the scaled variables tend to satisfy normality more often than the unscaled variables. Due to the lack of HOV (see Table 6) and non-normality of some of the scaled variables, we use Wilcoxon rank sum test to compare the variables for KO vs WT mice. See Table 7 for the corresponding p -values and direction of the alternatives. Comparing Tables 2 and 7, we see that after scaling most morphometric variables do not significantly differ between KO vs WT mice for Thin, Mushroom, Long Mushroom, and Stubby spines except for sL of Thin spines. But for Filopodia spines, KO mice have significantly larger sV , sSA , and sL , and smaller sD values compared to WT mice. That is, the scaled size for KO Filopodia spines is larger than WT Filopodia spines, and KO Filopodia spines are more similar in shape to the template.

We will run ANOVA on sD versus other scaled variables (i.e., sV , sSA , sL), Sc , spine, condition, mouse, and shaft type one at a time at each spine type level. See Figure 3 for the pair plots of the scaled variables. Observe that sD seems to be negatively correlated with sV , sSA , and Sc , while sV , sSA , and Sc are (mutually) positively correlated. First, to attain normality and lack of autocorrelation, we transform the scaled variables or remove outliers when necessary. See Table 8 for the transformations to render the scaled variables normal. The transformed variables can be assumed to be normal ($p_L > .05$ for each). Comparing Tables 3 and 8, we see that after scaling a smaller number of variables requires transformations to attain normality; furthermore, the transformations are less complicated.

To determine which variables significantly explain the variation in the scaled metric distances, we run a linear model with tsD being the response and each scaled variable is a predictor, one at a time. See Table 9 for the variables in decreasing order of significance with significant variables marked with an asterisk (*). We retain only the scaled variables that are significant at $\alpha = .05$ level, while others being discarded from the model. Observe that after scaling, no variable is significant in explaining the tsD for

Mushroom type spines, and the categorical variables are all non-significant except for mouse number for Thin spines. Furthermore, after scaling, the variables are less significant in explaining the variation in scaled distances; still tsV and $tsSA$ are best predictors for tsD .

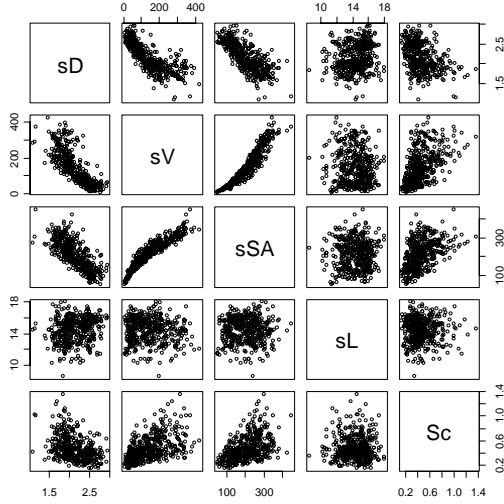


Figure 3: Pairs plot of the scaled morphometric measures together with Sc values with all spine types combined.

At each spine type category, we run a linear model for which tsD is the response variable, while all other variables that were found to be significant (see Table 9) with all possible interactions as predictor variables. Then we apply the same model selection procedure of Section 3.1 on this full model. The resulting models are presented in Table 10, where tsD_{ij} is the scaled distance for spine j for type i , μ_i is the overall mean for spines of type i , X_{ij}^{tsSA} is the $tsSA$ value for spine j of type i , X_{ij}^{tsV} is the tsV value for spine j of type i , β_i^{tsSA} is the slope for $tsSA$ value for spine type i , β_i^{tsV} is the slope for tsV for spine type i , $\beta_i^{tsVtsSA}$ is the slope for the interaction between X_{ij}^{tsV} and X_{ij}^{tsSA} (i.e., the product $X_{1j}^{tsV} \times X_{1j}^{tsSA}$), and \mathcal{E}_{ij} is the error term. The adjusted R^2 , p_{SW} , and p_{DW} values also provided in Table 10. Notice that normality of and lack of autocorrelation between errors are satisfied for each model. Furthermore, we see that $tsSA$ (shape component) and tV (scaled size

component) explain almost all of the variation in the scaled metric distances (e.g., 74 % for Thin dendrite spines).

4. Discussion and Conclusions

In this study, we investigate various morphometric measures, namely, metric distance, volume, surface area, length, and scale of dendrite spines of mice with two conditions (mice with a genetic modification designed to mimic a human neurological condition versus healthy mice) at different spine type levels which are based on pre-assigned shape categories.. We use the Large Deformation Diffeomorphic Metric Mapping algorithm to compute metric distances to measure morphometric differences between dendrite spines of mice. We compare the variances and distributions of these variables between the two mice conditions. We find that the healthy dendrite spines significantly differ in morphometry (size and shape) from the diseased spines. We also model the metric distances with respect to various other morphometric measures (such as volume, surface area, and length), and condition (healthy vs diseased) of spines. The morphometric measures significantly affect or explain the variation in the metric distances; so that in their presence the disease condition seem to not significantly affect the metric distances. But this does not mean that metric distances do not significantly differ with respect to the condition of mice, but rather metric distances are highly correlated with the other morphometric features, which ---when present in the model --- make the condition variable redundant. More precisely, morphometry of mice significantly differs due to the condition, but the variation in metric distances is mostly accounted for by the variation in other morphometric measures. We have also explored the effects of scaling on the morphometric measures and their relation to metric distances. We demonstrate that metric distances are highly dependent on the (scaled) morphometry of dendrite spines; and scaling changes the importance and order of this dependence. Therefore, computing metric distances with LDDMM is a powerful tool in detecting morphometric differences between dendrite spines of various sizes and shape; and scaling removes a considerable amount of the size influence so that the scaled distance becomes more of a measure of shape. However, in order to make scaling and within-spine type analysis more powerful (to detect the morphometric differences more specific to the condition) we recommend choosing a template for each spine type level, and then measuring the distances and scaling with respect to that spine for the spines of the same type as the template at each spine type level.

Acknowledgements

Research was supported by NSF ACS-9619020, NSF DMS-0456253, NSF DMS-0101329, NIH P41-RR15241, NIH P20-EB02013, P41-RR04050, P41-RR08605, R01-DA016602 and NSERC 31-611387.

5. References

- [1] G. Aldridge, T.N. Tasky, J.T. Ratnanather, M.E. Martone, M. Terada, M.F. Beg, L. Fong, E. Ceyhan, A.E. Kolasny, T. Brown, E.L. Cochran, S.J. Tang, D.V. Pisano, M. Vaillant, M.K. Hurdal, J.D. Churchill, W.T. Greenough, M.I. Miller, M.H. Ellisman, "Semi-automated shape analysis of dendrite spines from animal models of FragileX and Parkinson's Disease using Large Deformation Diffeomorphic Metric Mapping", Society for Neuroscience Annual Meeting, Washington DC, 2005. Available at <http://www.cis.jhu.edu/posters/sfn2005v2.pdf>
- [2] M.F. Beg, P.A. Helm, E. McVeigh, M.I. Miller, R.L. Winslow, "Computational Cardiac Anatomy Using MRI", *Magn Reson Med.*, 2004, 52(5): 1167-1174.
- [3] M.F. Beg, M.I. Miller, A. Trouvé, L. Younes, "Computing large deformation metric mappings via geodesic flows of diffeomorphisms", *International Journal of Computer Vision*, 2005, 61:139-157.
- [4] W.J. Burke, J.P. Miller, E.H. Rubin, J.C. Morris, L.A. Coben, J. Duchek, et al. "Reliability of the Washington University Clinical Dementia Rating", *Archives of Neurology*, 1988, 45:31-32.
- [5] K.P. Burnham and D. Anderson, *Model Selection and Multi-Model Inference*, New York: Springer, 2003.
- [6] G.E. Christensen, R.D. Rabbitt, M.I. Miller, "Deformable templates using large deformation kinematics", *IEEE Transactions on Image Processing*, 1996, 5:1435-1447
- [7] E. Ceyhan, R.Ç. Ölken, L. Fong, T.N. Tasky, M.K. Hurdal, M.F. Beg, M.E. Martone, J.T. Ratnanather, "Modeling Metric Distances of Dendrite Spines of Mice Based on Morphometric Measures", to appear in the *Proceeding of International Symposium on Health Informatics and Bioinformatics*, 2007.
- [8] W.J. Conover, *Practical Nonparametric Statistics*, 3rd ed. New York: John Wiley & Sons, 1993.
- [9] J.G. Csernansky, L. Wang, S.C. Joshi, J.T. Ratnanather, M.I. Miller, "Computational anatomy and neuropsychiatric disease: Probabilistic assessment of variation and statistical inference of group difference, hemispheric asymmetry, and time-dependent change", *NeuroImage*, 2004, 23:S56-S68.
- [10] P. Dalgaard, *Introductory Statistics with R*, Springer-Verlag, 2002.
- [11] A.C. Davison and D.V. Hinkley, *Bootstrap Methods and Their Application*, Cambridge Series in Statistical and Probabilistic Mathematics, 1997.
- [12] B. Everitt, *An R and S-Plus Companion to Multivariate Analysis*, Springer Texts in Statistics, 2005.
- [13] U. Grenander and M.I. Miller, "Computational anatomy: An emerging discipline", *Quarterly of Applied Mathematics*, 1998, 56:617-694.
- [14] K.M. Harris, F.E. Jensen, B. Tsao, "Three-dimensional structure of dendritic spines and synapses in rat hippocampus (CA1) at postnatal day 15 and adult ages: implications for the maturation of synaptic physiology and long-term potentiation", *J. Neurosci.*, 1992, 12, 2685-2705.
- [15] A. Khan, E. Aylward, P. Barta, M.I. Miller, M.F. Beg, "Semi-automated basal ganglia segmentation using large deformation diffeomorphic metric mapping", *Proceedings of International Conference on Medical Image Computing and Computer-Assisted Intervention: MICCAI*, 2005, 8(1):238-45
- [16] C.B. Kirwan, C. Jones, M.I. Miller, C.E.L. Stark, "High-resolution fMRI investigation of the medial temporal lobe", *Human Brain Mapping*, 2007, (in press).
- [17] B. Manly, *Multivariate Statistical Methods: A Primer*, 2nd ed: Chapman & Hall, 1994.
- [18] M.E. Martone, A. Gupta, M. Wong, X. Qian, G. Sosinsky, B. Ludäscher, M.H. Ellisman, "A cell-centered database for electron tomographic data", *Journal of Structural Biology*, 2002, 138, 145-155.
- [19] M.E. Martone, S. Zhang, A. Gupta, X. Qian, D.L. Price, M. Wong, S. Santini, M.H. Ellisman "The cell-centered database: a database for multiscale structural and protein localization data from light and electron microscopy", *Neuroinformatics*, 2003, 1: 379-395.
- [20] M.I. Miller, "Computational anatomy: Shape, growth, and atrophy comparison via diffeomorphisms", *NeuroImage*, 2004, 23:S19-S33.
- [21] M.I. Miller, M.F. Beg, C. Ceritoglu, C.E.L. Stark, "Increasing the power of functional maps of the medial temporal lobe using large deformation metric mapping", *Proc Natl Acad Sci. USA*, 2005, 102, 9685-9690.
- [22] M.I. Miller, G.E. Christensen, Y. Amit, U. Grenander, "Mathematical textbook of deformable neuroanatomies", *Proc Natl Acad Sci. USA*, 1993, 90:11944-11948.
- [23] M.I. Miller, C.E. Priebe, B. Fischl, A.E. Kolasny, Y. Park, R.L. Buckner, BIRN Morphometry (2006): Collaborative Computational Anatomy: The Perfect Storm for MRI Morphometry Study of the Human Brain via Diffeomorphic Metric Mapping, Multidimensional Scaling and Linear

Discriminant Analysis", *Proc Natl Acad Sci. USA*, 2007, (submitted).

[24] M.I. Miller, A. Trounev, L. Younes, "On the metrics and Euler-Lagrange equations of computational anatomy", *Annual Review of Biomedical Engineering*, 2002, 4:375-405.

[25] G.A.F. Seber and A.J. Lee, *Linear Regression Analysis*, New York: Wiley & Sons, 2003.

[26] H.C. Thode Jr., *Testing for Normality*, New York: Marcel Dekker, 2002.

[27] D.W. Thompson, *On Growth and Form: The Complete Revised Edition*, New York, Dover, 1992.

[28] P.M. Thompson, K.M. Hayashi, E.R. Sowell, N Gogtay, J.N. Giedd, J.L. Rapoport, et al., "Mapping cortical change in Alzheimer's disease, brain development, and schizophrenia", *Neuroimage*, 2004, 23:S2-S18.

[29] A.W. Toga, "Computational biology for visualization of brain structure", *Anatomy and Embryology*, 2005, 210:433-438.

[30] A.W. Toga and P.M. Thompson, "Brain atlases of normal and diseased populations", *Int Rev Neurobiol*, 2005, 66:1-54.

[31] S. Umeyama, "Least-Squares Estimation of Transformation Parameters Between Two Point Patterns", *IEEE Transactions on Pattern Analysis and Machine Intelligence*, 1991, 12(4): 376-380.

[32] L. Wang, M.F. Beg, J.T. Ratnanather, C. Ceritoglu, L. Younes, J.C. Morris, J.G. Csernansky, M. I. Miller, "Large Deformation Diffeomorphism and Momentum Based Hippocampal Shape Discrimination in Dementia of the Alzheimer Type", *IEEE Transactions on Medical Imaging*, 2006, (accepted).

6. TABLES

Variance Comparisons for KO vs WT at each spine type level for each variable					
	Thin	Mushroom	Filopodia	Long Mushroom	Stubby
D	.0006* (g)	.9546 (ℓ)	.9448 (g)	.1106 (ℓ)	.0022* (ℓ)
V	<.0001* (ℓ)	.4158 (ℓ)	.0450* (ℓ)	.0007* (ℓ)	.0566 (ℓ)
SA	<.0001* (ℓ)	.5998 (ℓ)	.0601 (ℓ)	.0051* (ℓ)	.0446* (ℓ)
L	<.0001* (ℓ)	.6193 (g)	.1254 (ℓ)	.1829 (ℓ)	.4966 (ℓ)
Sc	.0793 (g)	.2209 (g)	.6010 (g)	.8939 (g)	.7580 (g)

Table 1: The p -values for the HOV tests for spines of KO vs WT mice for each morphometric variable; (g) stands for KO>WT alternative and (ℓ) stands for KO<WT alternative.

Distributional Comparisons for KO vs WT at each spine type level for each variable					
	Thin	Mushroom	Filopodia	Long Mushroom	Stubby
D	.0001* (g)	.0356* (g)	.0013* (g)	.0161* (g)	.1835 (g)
V	<.0001* (g)	.0147* (g)	<.0001* (g)	.0058* (g)	.0132* (g)
SA	<.0001* (g)	.0206* (g)	<.0001* (g)	.0065* (g)	.0058* (g)
L	<.0001* (g)	.0113* (g)	.0145* (g)	.0179* (g)	.0311* (g)
Sc	<.0001* (ℓ)	.0343* (ℓ)	.0333* (ℓ)	.0219* (ℓ)	.0719 (ℓ)

Table 2: The p -values for Wilcoxon rank sum tests for spines of KO vs WT mice for each morphometric variable; (g) stands for KO>WT alternative and (ℓ) stands for KO<WT alternative.

Transformations of the variables at each spine type to attain normality.					
	Thin	Mushroom	Filopodia	Long Mushroom	Stubby
$tD =$	$\log(D)$	$\log(D)$	$\log(D)$	$\log(D)$	$\log(D)$
$tV =$	$\sqrt[4]{\log(V)}$	$\log(V)^3$	$\log(V)$	$\log(V)$	$\log(V)$
$tSA =$	$\log(SA)$	$\log(SA)^3$	$\log(SA)$	$\log(SA)$	$\log(SA)$
$tL =$	$\log(L)^2$	$\sqrt[4]{L}$	$\sqrt[5]{\log(L)}$	$\log(L)$	L
$tSc =$	$\log(1/Sc)$	$1/Sc$	$\log(1/Sc)$	$\log(1/Sc)$	Sc

Table 3: Transformations of the variables at each spine type to attain normality.

(Transformed) variables in ANOVA F -test to explain variation in tD values at each spine type level								
Type	Variables							
Thin	tSA^*	tV^*	tSc^*	tL^*	cond*	mouse*	shaft*	spine*
Mushroom	tV^*	tSA^*	tSc^*	tL^*	cond	mouse	spine	shaft
Filopodia	tV^*	tSA^*	cond*	tL^*	tSc^*	mouse*	shaft	spine
Long Mushroom	tSA^*	tV^*	tSc^*	tL^*	cond*	mouse	shaft	spine
Stubby	tSc^*	tV^*	tSA^*	tL^*	mouse	cond	spine	shaft

Table 4: The variables for the ANOVA F -tests for tD vs other (transformed) variables one at a time. The significant variables at .05 level are marked with an asterisk (*) and the variables are sorted in decreasing order of significance (from left to right).

Spine Type	Model	Adj. R^2	p_{SW}	p_{DW}
Thin	$tD_{1j} = \mu_1 + \beta_1^{tSA} X_{1j}^{tSA} + \beta_1^{tSc} X_{1j}^{tSc} + \varepsilon_{1j}$.48	<.0001	.3761
Mushroom	$tD_{2j} = \mu_2 + \beta_2^{tV} X_{2j}^{tV} + \varepsilon_{2j}$.82	.3363	.6698
Filopodia	$tD_{3j} = \mu_3 + \beta_3^{tV} X_{3j}^{tV} + \varepsilon_{3j}$.61	.1099	.4472
Long Mushroom	$tD_{4j} = \mu_4 + \beta_4^{tSA} X_{4j}^{tSA} + \varepsilon_{4j}$.85	.2430	.8880
Stubby	$tD_{5j} = \mu_5 + \beta_5^{tSc} X_{5j}^{tSc} + \varepsilon_{5j}$.70	.2092	.3480

Table 5: The models to explain the variation in tD values at each spine type category.

Variance Comparisons for KO vs WT at each spine type level for each scaled variable					
	Thin	Mushroom	Filopodia	Long Mushroom	Stubby
sD	.3004 (ℓ)	.3181 (ℓ)	.8059 (ℓ)	.1353 (g)	.3891 (ℓ)
sV	.2637 (g)	.6818 (ℓ)	.0735 (ℓ)	.1218 (g)	.0039* (ℓ)
sSA	.8509 (g)	.2435 (ℓ)	.0194* (ℓ)	.4872 (g)	.0060* (ℓ)
sL	.0201* (g)	.8569 (g)	.0332* (g)	.4107 (ℓ)	.9930 (ℓ)

Table 6: The p -values for the B-F HOV tests for spines of KO vs WT mice for each scaled morphometric variable.

Distributional Comparisons for KO vs WT at each spine type level for each scaled variable					
	Thin	Mushroom	Filopodia	Long Mushroom	Stubby
sD	.4680 (ℓ)	.4192 (ℓ)	.0145* (ℓ)	.2851 (ℓ)	.4245 (ℓ)
sV	.4005 (g)	.1612 (g)	.0091* (g)	.3997 (g)	.3617 (g)
sSA	.1754 (g)	.2387 (g)	.0004* (g)	.2985 (g)	.2142 (g)
sL	.0016* (g)	.1382 (g)	.0392* (g)	.3263 (g)	.1190 (ℓ)

Table 7: The p -values for the Wilcoxon rank sum tests for spines of KO vs WT mice for each scaled morphometric variable.

Transformations of the scaled variables at each spine type to attain normality.					
	Thin	Mushroom	Filopodia	Long Mushroom	Stubby
$tsD =$	$\sqrt[4]{sD}$	sD^2	$\log(sD)$	sD	sD
$tsV =$	$\sqrt[4]{sV}$	sV	sV	$\sqrt{\log(sV)}$	\sqrt{sV}
$tsSA =$	$\log(sSA)^5$	sSA	$\log(sSA)$	sSA	\sqrt{sSA}
$tsL =$	sL^4	sL	sL^3	sL	sL

Table 8: Transformations of the scaled variables at each spine type to attain normality.

(Transformed) scaled variables significant in ANOVA F -test to explain variation in tsD values at each spine type level								
Type	Variables							
Thin	tsV^*	$tsSA^*$	tSc^*	mouse*	shaft	tsL	spine	Cond
Mushroom	mouse	cond	tsL	tSc	tsV	shaft	spine	tsSA
Filopodia	tsV^*	$tsSA^*$	cond	mouse	tSc	tsL	spine	shaft
Long Mushroom	tsV^*	$tsSA^*$	spine	tSc	tsL	cond	mouse	shaft
Stubby	$tsSA^*$	tsV^*	tSc	mouse	tsL	spine	cond	shaft

Table 9: The variables for the ANOVA F -tests for tsD vs other (transformed) scaled variables one at a time. The significant variables at .05 level are marked with an asterisk (*), and the variables sorted in decreasing order of significance (from left to right).

Spine Type	Model	Adj. R^2	p_{SW}	p_{DW}
Thin	$tsD_{1j} = \mu_1 + \beta_1^{tsV} X_{1j}^{tsV} + \beta_1^{tsSA} X_{1j}^{tsSA} + \beta_1^{tsVtsSA} X_{1j}^{tsV} \times X_{1j}^{tsSA} + \epsilon_{1j}$.74	.2473	.1054
Mushroom	$tsD_{2j} = \mu_2 + \epsilon_{2j}$	NA	.5537	.4754
Filopodia	$tsD_{3j} = \mu_3 + \beta_3^{tsV} X_{3j}^{tsV} + \epsilon_{3j}$.36	.3266	.7741
Long Mushroom	$tsD_{4j} = \mu_4 + \beta_4^{tsV} X_{4j}^{tsV} + \beta_4^{tsSA} X_{4j}^{tsSA} + \epsilon_{4j}$.60	.8268	.4061
Stubby	$tsD_{5j} = \mu_5 + \beta_5^{tsSA} X_{5j}^{tsSA} + \epsilon_{5j}$.31	.9174	.5882

Table 10: The models to explain tsD values at each spine type category.